PERGAMON

International Journal of Heat and Mass Transfer 41 (1998) 3589–3609

International Journal of HEAT and MASS TRANSFER

Effect of contaminant properties and temperature gradients on the efficiency of transient gaseous contaminant removal from an enclosure : a numerical study

M. Soria*, A. Oliva, M. Costa, C. D. Pérez-Segarra

Laboratori de Termotècnia i Energètica, Departament de Màquines i Motors Tèrmics, Universitat Politènica de Catalunya, Colom, 11, 08222 Terrassa, Barcelona, Spain

Received 7 June 1997 ; in final form 10 November 1997

Abstract

This paper reports the results of a numerical study on the transient removal of a contaminant from a two-dimensional enclosure with one inlet and one outlet. The influence of buoyancy forces due to thermal and concentration gradients, contaminant diffusivity, inlet velocity and outlet disposition over the cleaning-time are studied. The governing equations of the laminar flow (continuity, momentum, energy and contaminant concentration) are solved by means of the SIMPLEC algorithm. Several simulations of the same test case have been made, using two numerical schemes : PLDS and SMART, in order to determinate which one provides better performances. For isothermal situations, the time required to remove the contaminant is studied parametrically as a function of the outlet position and the governing dimensionless numbers (Reynolds number, Schmidt number and solutal Rayleigh number), while the effect of horizontal temperature differences is studied in several situations in which it plays an important role. Buoyancy forces are found to have a strong influence over the flows and, in consequence, over the cleaning times.

Nomenclature

c mass concentration
C dimensionless concentration, $(c_0-c)/\Delta c$
D mass diffusivity of pollutant
DF direct flow (inlet and outlet placed at the top of the cavity, Fig. 1)
g gravitational acceleration
h dimensional width of inlet and outlet ports, $H/10$
H dimensional height of the enclosure
IF indirect flow (inlet at the top and outlet at the bottom of the cavity, Fig. 1)
L dimensional length of the enclosure, $2H$
Le Lewis number, α/D
n direction normal to the boundary
nx, ny number of control volumes in x and y axes
p_d dynamic pressure
P dimensionless pressure, $p_d/(\rho\alpha^2/H^2)$
Pr Prandtl number, v/α
Ra_S solute Rayleigh number, $\beta_S\Delta cH^3g/\alpha v$
Ra_T thermal Rayleigh number, $\beta_T\Delta\theta H^3g/\alpha v$
Re Reynolds number, hu_{in}/v
Sc Schmidt number, v/D
t dimensional time
T dimensionless temperature, $(\theta-\theta c)/\Delta\theta$
u, v dimensional horizontal and vertical velocities
U, V dimensionless horizontal and vertical velocities, $U=u/(\alpha/H)$, $V=v/(\alpha/H)$
x, y dimensional coordinates
X, Y dimensionless coordinates $X=x/H$, $Y=y/H$.

Greek symbols

α thermal diffusivity
β_T thermal volumetric expansion coefficient, $-(1/\rho)\cdot(\partial\rho/\partial\theta)$
β_S mass volumetric expansion coefficient, $-(1/\rho)\cdot(\partial\rho/\partial c)$
Δc increment of concentration used as a reference, c_0-c_{in}

* Corresponding author.

0017–9310/98 $19.00
PII : S0017–9310(97)00366–9

$\Delta\theta$ increment of temperature used as a reference, $\theta_c - \theta_h$
$\Delta\tau^*$ time step expressed in the air-renovation scale
η_d displacement efficiency
θ dimensional temperature
θ_c, θ_h cold and hot dimensional reference temperatures
ν kinematic viscosity
ρ density
τ dimensionless time, $t/(H^2/\alpha)$
τ^* number of air renovations, $tu_{in}h/(LH)$
$\tau^*_{C_{min}}$ number of air renovations required to reach $C_{min} = 0.95$
$\tau^*_{C_{avg}}$ number of air renovations required to reach $C_{avg} = 0.95$.

Subscripts
avg average
in inlet
l left wall
min minimum
out outlet
r right wall
0 initial value.

1. Introduction

Gaseous combustibles have many attractive features for their use in domestic and industrial environments, but their intrinsic danger is a serious limitation to their use. The purpose of this work is to study numerically an idealized gas transport situation after an accidental leak in order to provide a better knowledge of the influence of gas properties (density and diffusivity) and room airflow on the time required to reach safe conditions.

In usual room airflow conditions, where the expected concentrations of contaminants are small, the buoyancy forces generated by concentration gradients can be neglected. Two typical examples of these conditions are: the airflow in an air conditioned building and the airflow in a clean room. In the first case the problem is to provide [1] and acceptable microclimate (thermal environment and air quality) in the space being ventilated, and in the second, to provide both a low concentration of airborne particles and a low air turbulence. There are many numerical and experimental studies addressed to provide information on the indoor airflows in both cases. A few examples of these studies in both areas are given below.

Fang and Grot [2] simulated numerically the turbulent flow emerging from an air diffuser in an idealized air conditioned room, taking into consideration the buoyancy effects due to thermal gradients in order to obtain information for the design of indoor ventilation systems. Murakami et al. [3] analyzed the airflow in an idealized clean room with obstacles, by means of model experiments and three-dimensional numerical simulations, in order to evaluate the transport of a scalar quantity with no effect over the momentum equations. Kato et al. [4] studied numerically flow and contaminant fields in a room with both the exhaust and supply openings at the ceiling, installed in such a way that the airflow rates are balanced locally, in order to avoid the formation of recirculation areas in the whole room.

Considering a problem similar to ours, but assuming that the fluid density was nearly constant (independent of contaminant concentration), Lage et al. devoted two works to the study of the transport of a contaminant from an enclosure. In the first one [5] they supposed a uniform contaminant distribution at the beginning of the process and studied its transient removal. They performed numerical simulations for a fixed Sc number and a wide range of Re numbers and four dispositions of the inlet and the outlet, finding a compact expression to predict the average concentration after a large number of air renovations. Later [6], for a similar enclosure, they studied the removal of a contaminant being steadily generated by a concentrated source placed at a point inside the enclosure, assuming that the source mass flow rate was negligible compared with the inlet mass flow rate. They studied the maximum concentration and the number of air renovations required to reach it for several *Re* numbers, contaminant source placements, inlet and outlet dispositions. They found an inlet/outlet optimal disposition for each source location that can enhance significantly the transport process.

The main difference between the present work and the aforementioned is that in this case, after the leak, high gas concentrations can be found, and the buoyancy forces generated by concentration gradients can significantly affect the flows, and consequently, the cleaning times.

In this paper a more general case is considered where both temperature and concentration gradients influence the flow (double-diffusion convection).

Double diffusive convection is an important phenomena in many areas, like material processing, atmospheric flows, transport of contaminants of oceanography and many studies have been made on this subject. The simultaneous action of temperature and concentration gradients causes the flow to be more complex, specially in the cases where Le number, the quotient of both diffusivities (α/D), is high. A number of numerical studies are addressed to this area. For instance: Gebhart and Pera [7] were among the first to study numerically the double-diffusion phenomena in vertical laminar motions along surfaces and in plumes; special attention was paid to the influence of dimensionless parameters relevant to double diffusion and to heat and mass transfer rates. Bergman and Ungan [8] investigated numerically and experimentally the double-diffusive convection induced by bottom heating with a finite heated strip placed beneath a salt stratified layer. Lee and Hyun devoted two papers [9, 10] to the numerical study of the transient behaviour of a vertical cavity with combined opposing and coop-

erating horizontal temperature and concentration gradients. The resulting transient flows were analyzed for different buoyancy ratios. In both cases, the formation of a multilayered flow was observed. Later, in a similar situation, Han and Kuehn studied experimentally [11] and numerically [12] the double diffusive natural convection fluid flow in a vertical cavity with horizontal temperature and concentration gradients imposed. Weaver and Viskanta devoted two works [13, 14] to the investigation of the heat and mass transfer in a cavity due to natural convection driven by combined thermal and solute bouyancy forces. The first one is addressed to the study of the effects of variable thermophysical properties while the second one examines the influence of species interdiffusion, Soret and Dufour effects. Kamakura and Ozoe [15] studied numerically and experimentally the transient formation and destruction of multi-layered roll cells in cavities initially filled with a solution having a linear concentration profile and later subjected to a horizontal temperature gradient. Béghein et al. [16], in a work that, for the boundary conditions specified, can be considered as a generalization of the well-known thermal driven cavity problem, simulated the steady-state flow of air mixed with a pollutant in a closed square cavity subjected to horizontal temperature and concentration gradients, in a range of dimensionless parameters that roughly corresponds to the ones selected in this paper.

The present study examines numerically the transient effects that the buoyancy forces due to concentration and temperature gradients have over the time required to remove a uniformly distributed contaminant from an enclosure with one inlet and one outlet. The effects of different contaminant diffusivities (*Sc* numbers), *Re* numbers and outlet dispositions are also investigated. The governing equations of the flow are solved using a pressure-based method. The flow is considered to be two dimensional and laminar. Although three-dimensional effects are known to be of importance in some flow configurations [17, 18], a two-dimensional model retains a description of the main interest aspects and make feasible to perform enough transient simulations as to draw conclusions. The study of turbulent flows would require the introduction of turbulence models like the two equation k–ε turbulence model [19, 20].

2. Physical model and numerical aspects

2.1. Model equations

The double-diffusion model here considered assumes two-dimensional laminar flow, both fluids (air and contaminant) to be perfectly mixible, and the Soret, Dufour and species interdiffusion effects [14, 21] negligible. All the physical properties are supposed to be independent of the temperature and concentration, except the density variations, for which the Boussinesq approximation is used.

The set of equations that describes the flow (continuity, momentum, energy transport and mass transport) can be expressed in dimensionless form as follows:

$$\frac{\partial U}{\partial X}+\frac{\partial V}{\partial Y}=0 \tag{1}$$

$$\frac{\partial U}{\partial \tau}+U\frac{\partial U}{\partial X}+V\frac{\partial U}{\partial Y}=-\frac{\partial P}{\partial X}+Pr\left(\frac{\partial^2 U}{\partial X^2}+\frac{\partial^2 U}{\partial Y^2}\right) \tag{2}$$

$$\frac{\partial V}{\partial \tau}+U\frac{\partial V}{\partial X}+V\frac{\partial V}{\partial Y}=-\frac{\partial P}{\partial Y}+Pr\left(\frac{\partial^2 V}{\partial X^2}+\frac{\partial^2 V}{\partial Y^2}\right)+Pr(Ra_{\mathrm{T}}T-Ra_{\mathrm{S}}C) \tag{3}$$

$$\frac{\partial T}{\partial \tau}+U\frac{\partial T}{\partial X}+V\frac{\partial T}{\partial Y}=\frac{\partial^2 T}{\partial X^2}+\frac{\partial^2 T}{\partial Y^2} \tag{4}$$

$$\frac{\partial C}{\partial \tau}+U\frac{\partial C}{\partial X}+V\frac{\partial C}{\partial Y}=\frac{Pr}{Sc}\left(\frac{\partial^2 C}{\partial X^2}+\frac{\partial^2 C}{\partial Y^2}\right). \tag{5}$$

The dimensionless values used are:

$$(X,Y)=(x,y)/H,\quad (U,V)=(u,v)/(\alpha/H),\quad \tau=t/(H^2/\alpha) \tag{6}$$

$$C=(c_0-c)/\Delta c,\quad T=(\theta-\theta_{\mathrm{c}})/\Delta\theta \tag{7}$$

$$P=p_{\mathrm{d}}/(\rho\alpha^2/H^2) \tag{8}$$

$$Pr=\nu/\alpha,\quad Sc=\nu/D \tag{9}$$

$$Ra_{\mathrm{S}}=\beta_{\mathrm{S}}\Delta c H^3 g/\alpha\nu,\quad Ra_{\mathrm{T}}=\beta_{\mathrm{T}}\Delta\theta H^3 g/\alpha\nu. \tag{10}$$

The reference increments of temperature and concentration are:

$$\Delta c=c_0-c_{\mathrm{in}},\quad \Delta\theta=\theta_{\mathrm{c}}-\theta_{\mathrm{h}}. \tag{11}$$

This set of equations (1)–(5) presents relevant differences with the standard pure thermal natural convection equations. Firstly, there are two scalar transport equations, the energy (4) and the mass transport (5). These equations are formally identical, except for a different dimensionless diffusivity. The quotient Pr/Sc can also be expressed as $1/Le$, where Le is the ratio between thermal and mass diffusivities. For liquid solutions, thermal diffusivity is considerably higher than mass diffusivity, and this is one of the causes of many remarkable patterns of these flows, like convective cells separated by sharp interfaces [9–12, 15]. For air mixtures, Gebhart and Pera [7] pointed out that the chemical species of most common interest have *Sc* numbers in the range 0.1–10. In this study, values of *Sc* between 0.25 and 2.0 have been considered, while *Pr* has been fixed to be 0.71.

Secondly, the vertical momentum equation (3) is coupled with all the rest of the set, including the mass transport equation, due to the different density of the contaminant. In some cases the effects of buoyancy due to concentration gradients can be important; for

instance, as Gebhart and Pera [7] showed, for air saturated of water vapor at 20°C and for a temperature difference of 10°C, the buoyancy forces due to the concentration differences are about three times stronger than the buoyancy forces due to the temperature differences. In our case, the density of the contaminant and its initial and inlet concentrations determine the Ra_S number. While Ra_T is always positive, Ra_S can be either positive or negative.

2.2. Estimations of concentration, time and transport efficiency

By dividing the dimensional time t by the reference value $LH/u_{in}h$ we obtain τ^* which represents the number of air renovations. This value has been used as a time scale in order to present the results.

Two characteristic values of the gaseous concentration at a given instant are used, the displacement efficiency η_d, defined by Anderson and Mehos [22] as $\eta_d = (c_0 - c_{avg})/\Delta c$, and the maximum stress concentration c_{max}, values that, according to the definition of the dimensionless concentration C are, respectively, equal to C_{avg} and C_{min}.

The efficiency of the whole transport process can be established with two dimensionless times, $\tau^*_{C_{min}}$ and $\tau^*_{C_{avg}}$, defined as the number of air renovations required to reduce the minimum and average concentrations up to a 95% of the final value ($C = 0.95$). This value can be chosen in a rather arbitrary way, depending on the final application. For instance, Lage et al. [5, 6] used a higher one, 0.99999.

2.3. Physical domain. Boundary and initial and conditions

The cavity studied, represented in Fig. 1 is rectangular, with one inlet and one outlet. While the inlet is always at the top of the cavity, two outlet positions have been considered: the one presented in the left part of the figure, hereafter called DF, which stands for direct flow, and a second one in the right part, hereafter called IF, for indirect flow. The geometric aspect ratios L/H and h/H have been fixed to 2 and 0.1, respectively.

The velocity boundary conditions are of non-slip, except in the inlet and outlet flow sections, where a dimensionless normal velocity U_{in} is prescribed as follows:

$$U_{in} = Re\,Pr\,H/h \tag{12}$$

where Re is an inlet-width based Reynolds number,

$$Re = hu_{in}/v. \tag{13}$$

In the energy equation the horizontal boundaries are always supposed to be adiabatic. Isothermal vertical walls at T_l (left wall) and T_r (right wall) are considered. The temperature at the inlet is fixed to be T_{in} and at the outlet $\partial T/\partial n = 0$ has been imposed.

In the concentration equation (5) a null gradient is used everywhere except at the inlet, where C is fixed to 1. For clarity, it should be noted that this value corresponds to the dimensional value of the external air.

Lage et al. in their aforementioned works, after considering the effect of different outlet boundary conditions pointed out that even for very low Re number flows, the error introduced by the assumption of $\partial C/\partial n = 0$ is irrelevant, so the same boundary condition has been used here for C and T equations.

2.4. Isothermal flow conditions

The vertical walls and the inlet are fixed at the same temperature ($T_{in} = T_l = T_r = 0$). The initial conditions are: $U_0 = V_0 = C_0 = T_0 = 0$ (isothermal and uniformly contaminated air). As there is no temperature gradient, the buoyancy effects are only due to concentration gradients.

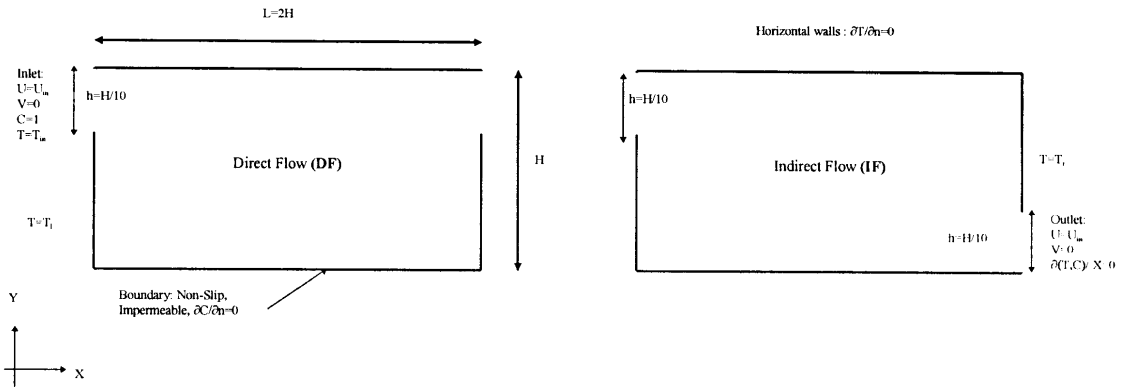

Fig. 1. The cavity and boundary conditions under consideration. Different velocity and temperature initial conditions are investigated, but in all the cases, the cavity is considered to be initially uninformly filled with a $c = c_0$ gas, corresponding to a dimensionless value $C = 0$.

2.5. Non-isothermal flow conditions

The effect of an externally imposed horizontal temperature difference has been studied. For the same Ra_T number, two different boundary conditions have been considered: negative temperature difference, $T_{in} = T_l = 1$, $T_r = 0$, and positive temperature difference $T_{in} = T_l = 0$, $T_r = 1$.

Two different initial conditions have been considered. In the first situation, referred as steady, initially the cavity is supposed to be uniformly contaminated ($C_0 = 0$) and subjected to a temperature gradient imposed a long time ago. The permanent state has been reached, and at the beginning of the transport process, there are steady non-zero velocity, pressure and temperature fields due to the thermal driven natural convection process. These fields depend on the Ra_T number and on the sign of the temperature difference. In the second situation, referred as static, initially the conditions are $U_0 = V_0 = T_0 = C_0 = 0$, and suddenly the left or right wall temperature is supposed to increase up to 1 (i.e., $T_l = 1$ and $T_r = 0$ or $T_l = 0$ and $T_r = 1$).

2.6. Numerical algorithm and validation of the software

The SIMPLEC algorithm [23] was used to integrate the set of governing equations. The first and second order numerical schemes PLDS (Power Law Difference Scheme) [24] and SMART [25] have been used. After a set of tests later discussed, SMART was chosen for its better performance. The dimensionless $\Delta\tau^*$ was kept constant during all the simulation. The resulting set of algebraic equations were solved with the MSIP [26] algorithm. At each time step, iterations were stopped when the three following conditions were simultaneously satisfied:

$$abs(C_{avg}\text{ iteration } j - C_{avg}\text{ iteration } j-1) < 10^{-6}$$

$$abs(T_{avg}\text{ iteration } j - T_{avg}\text{ iteration } j-1) < 10^{-6}$$

$$max(\text{mass error})/(u_{in}h) < 10^{-11}.$$

The natural convection benchmark case proposed by De Vahl Davis [27] was used to check the correctness of the results provided by the program, using different non-uniform grids generated with the following function:

$$Vclx(i) = \frac{1}{2}\frac{atan\left(\xi \cdot \left(\frac{2i}{n} - \left(1 + \frac{2}{n}\right)\right)\right)}{atan(\xi)}.$$

Here, ξ is a concentration parameter, n is the number of control volumes ($n = nx = ny$), i takes integer values from 1 to $n+1$ and $Vclx(i) = Vcly(i)$ are the border lines between control volumes for x and y axes. Ra_T numbers between 10^3 and 10^6 were tested, keeping $Pr = 0.71$. For $Ra_T = 10^6$ and $\xi = 2$ the results obtained are presented in Table 1. These concentration functions and factors were found to provide a good value of the average Nusselt number with $Ra_T = 10^6$ and a 42×42 grid, and it was used in the rest of the grids without further investigation.

Table 1
Results obtained in the thermal-driven square cavity problem

	Vahl Davis	42×42	82×82	160×160
Nu_{avg}	8.800	8.844	8.825	8.829
U_{max}	64.63	65.50	65.04	64.87
Y–U_{max}	0.850	0.854	0.855	0.852
V_{max}	219.36	221.19	220.79	220.56
X–V_{max}	0.0379	0.0348	0.0386	0.0382
Nu_{max}	17.925	18.046	17.655	17.573
Y–Nu_{max}	0.0378	0.0348	0.0386	0.0382
Nu_{min}	0.989	1.07	1.01	0.98
Y–Nu_{min}	1	1	1	1

Nu_{avg} is the mean Nusselt at the vertical walls. U_{max}, Y–U_{max}, V_{max} and X–V_{max} are, respectively, the maximum dimensionless velocities at the central vertical and horizontal planes and their dimensionless positions. Nu_{min} and Y–Nu_{min} are the minimum Nusselt number at the vertical cold wall and its dimensionless position. A complete description of this case and the values listed here can be found in [27].

In order to ensure the correctness of transient simulations, a case presented by Fu et al. [28] was reproduced using a $n = 42$, $\xi = 2$ grid. In this case, a square cavity is subjected to a horizontal temperature gradient and when the steady state is reached, the temperature at the hot wall suddenly decreases to be equal to the cold one. In Fig. 2, the average Nusselt numbers at both walls have been represented against the dimensionless time. As can be seen, good agreement has been obtained.

In order to check the concentration equation correctness, some of the aforementioned test cases were repeated imposing $Sc = Pr$ and fixing Ra_S to take the value of Ra_T and Ra_T to be 0, along with analogous dimensionless boundary conditions. The same results were obtained replacing C by T.

2.7. Tests of grid independence: time step and grid size

In this section, differences in C_{min} have been used as a representative measure because C_{min} is the value of main interest in this work, and because it reflects better than C_{avg} differences in the numerical procedure.

The appropriate time step and grid size were selected after several numerical accuracy tests. The grid sizes tested ranged between 20×10 (number of control volumes) and 200×100 and the time steps ($\Delta\tau^*$) between 10^{-3} and 5×10^{-4}.

In general, like in the example of Fig. 3 (top), the value of $\Delta\tau^* = 4 \times 10^{-3}$ has been used to obtain a reasonably

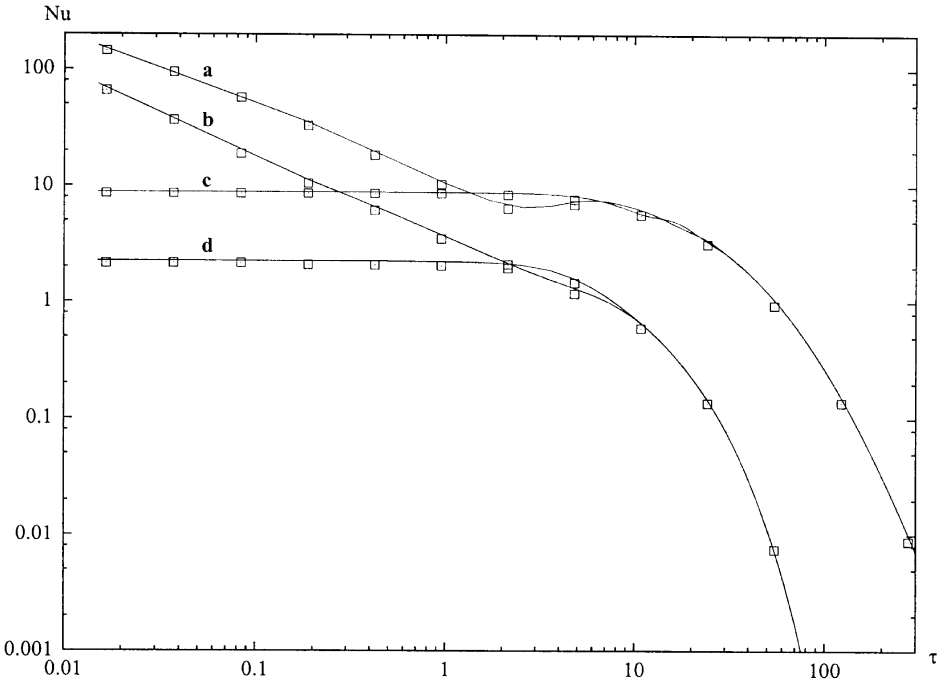

Fig. 2. Comparison between present results (solid line) and Fu et al. results (square dots). Average Nu numbers at both walls. (a) Left wall, $Ra_T = 10^6$; (b) left wall, $Ra_T = 10^4$; (c) right wall, $Ra_T = 10^6$; (d) right wall, $Ra_T = 10^4$.

accurate result. In certain situations, like the one shown in Fig. 3 (bottom), in which an abrupt change in the slope of C_{min} appears, or in the highest Re values considered, $\Delta\tau^* = 5 \times 10^{-4}$ has been used.

In order to find a solution as near as possible to the grid-independent one, several runs of a test case (isothermal; $Ra_S = -7 \times 10^4$; IF; $Sc = 1$; $Re = 30$) were made with uniform grids of different sizes but the same aspect ratio, 2×1, using PLDS and SMART schemes. To summarize all the transient evolution with a single number, the value of C_{min} at a certain τ^* has been chosen. An early value was selected, $\tau^* = 1.2$. Later, as $C_{min}(\infty) = 1$, the differences of the values obtained with different grids and numerical schemes tend to vanish.

The results are presented in Fig. 4. It can be seen that both schemes converge to the same value, that seems to be close to the 200×100 result. For the same grid size, SMART provides more accurate values, specially for the coarser grids, but unfortunately, it spends more CPU time. Grids of other aspect ratios have been tested and found to provide results converging to the same value but slower, so their use was not considered.

In order to decide if it was better to use a coarser grid and SMART, or a finer one and PLDS, an error measure was introduced as

$$\text{Error} = 100.\, abs(C_{min}(\tau^* = 1.2) - \text{Bestvalue})$$

where Bestvalue corresponds to the result obtained with a grid of 200×100 and SMART scheme.

This error was represented in Fig. 4 (bottom) against the CPU time needed to reach $\tau^* = 1.2$, expressed in CPU minutes of a workstation HP735. The CPU times obtained depend strongly on the degree of optimization of a particular program, but the ratio between PLDS and SMART CPU times is expected to remain approximately constant for other programs and computers.

After these tests we can conclude that, in the situation considered, for the same grid size, PLDS is between 1.3 and 2.5 times faster than SMART, but also less accurate, specially for the coarser grids considered; on the other hand, for a given CPU time, SMART provides more accurate results.

All these considerations led us to the election of SMART scheme and a grid of 80×40 uniformly-disposed control volumes for all cases. This option provides results that, in the aforementioned test case, differ less than 0.7% from the best value obtained.

It could be argued that faster results with the same or more accuracy might be obtained with coarser non-uniform grids. However in the range of situations considered, many different flows are expected to be found,

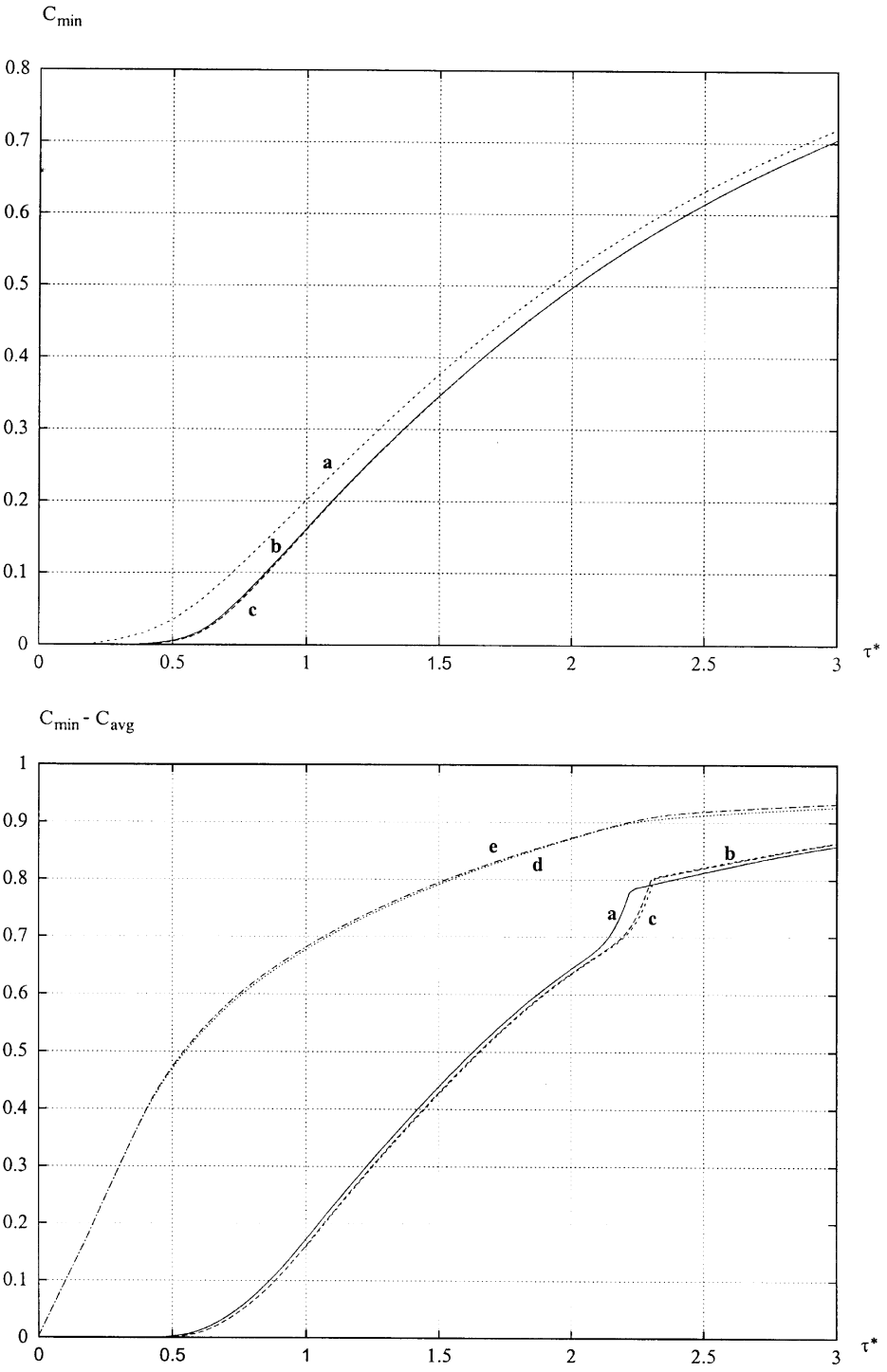

Fig. 3. Numerical accuracy tests. Effect of time step over the simulation of two test cases. (top): IF, $Re = 30$, isothermal, $Ra_S = 7 \times 10^4$, $Sc = 1$, (a) C_{min} vs τ^*, $\Delta\tau^* = 10^{-1}$; (b) C_{min} vs τ^*, $\Delta\tau^* = 4 \times 10^{-3}$; (c) C_{min} vs $\Delta\tau^* = 10^{-3}$. (bottom): DF, $Re = 30$, isothermal, $Ra_S = 3.5 \times 10^4$, $Sc = 2$. (a) C_{min} vs τ^*, $\Delta\tau^* = 4 \times 10^{-3}$; (b) C_{min} vs τ^*, $\Delta\tau^* = 10^{-3}$; (c) C_{min} vs τ^*, $\Delta\tau^* = 5 \times 10^{-4}$; (d) C_{avg} vs τ^*, $\Delta\tau^* = 4 \times 10^{-3}$; (e) C_{avg} vs τ^*, $\Delta\tau^* = 5 \times 10^{-4}$.

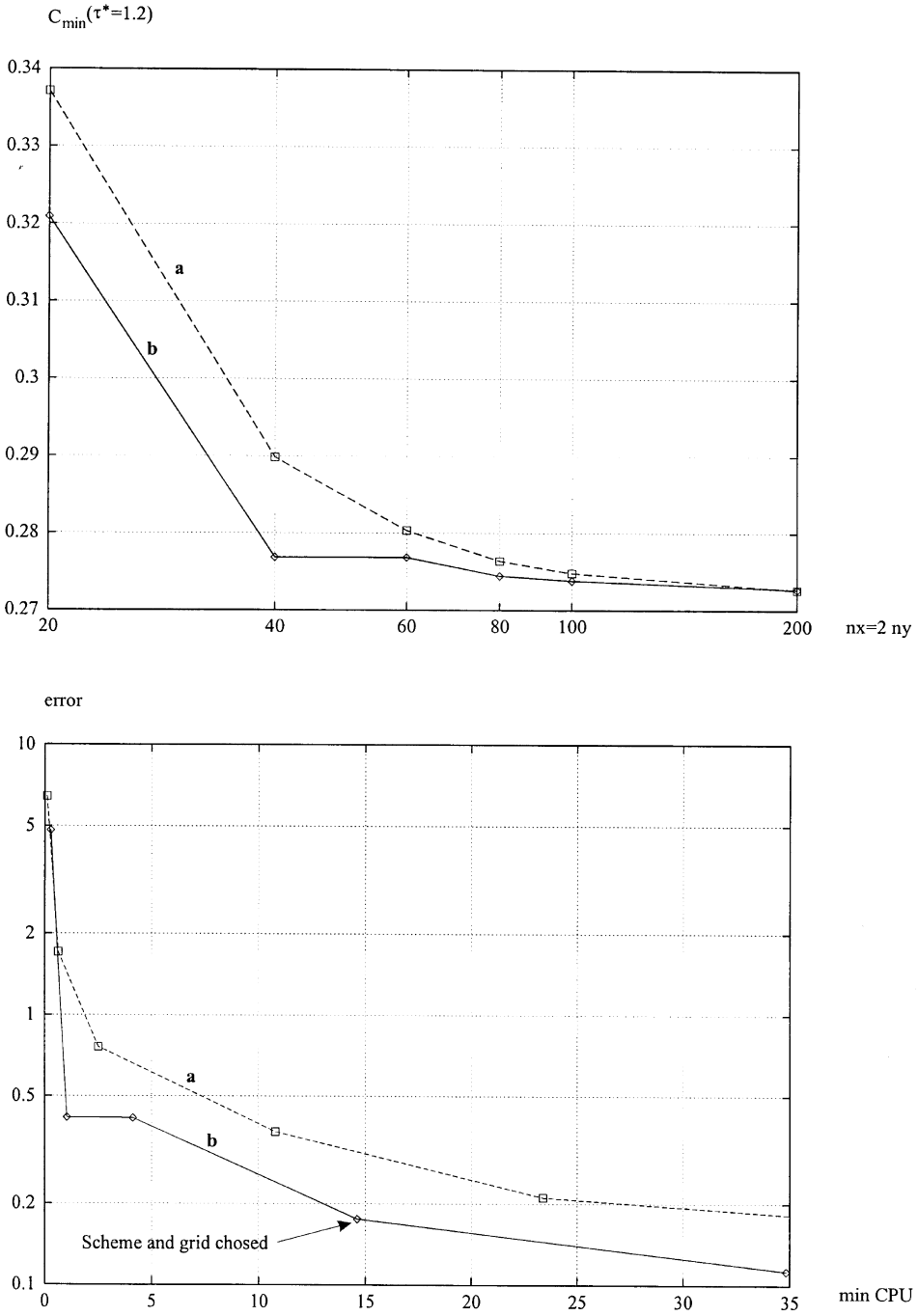

Fig. 4. Numerical accuracy tests. Effect of grid size and numerical scheme over a test case: IF, $Re = 30$, isothermal, $Ra_S = -7 \times 10^4$, $Sc = 1$. (a) PLDS; (b) SMART. (top) $C_{min}(\tau^* = 1.2)$ for different grid sizes and SMART/PLDS numerical schemes. (bottom) Error = 100. *abs* ($C_{min}(\tau^* = 1.2) -$ Bestvalue) obtained as a function of CPU time for different grid sizes and SMART/PLDS numerical schemes.

and the CPU time required to optimize each situation could easily have been greater than the extra CPU time spent using uniform, non-optimal grid dispositions.

After the comparison of the predictions made by the numerical code against the results of other authors and the study of grid sizes and time steps required to reach accurate solutions in the range of dimensionless values that are here under consideration, we can conclude that the numerical code can be used for the numerical experimentation of the behaviour of physical systems described by the set of governing equations (1)–(5), i.e., systems in which the hypothesis stated in Section 2.1 are valid.

However, as there is no published experimental data referent to transient double-diffusive flows in opened cavities (to the knowledge of the authors), two reasons justify the need of experimental measures: (i) check the validity of the hypothesis stated in Section 2.1; (ii) extend the present study to higher Re, Ra_S and Ra_T numbers, where turbulence modeling would be required and experimental measures would be needed to validate the turbulence models in these double diffusive flows.

3. Isothermal situations

If we consider isothermal flow situations with a fixed Pr number, the history of the flow depends on the geometrical disposition (DF or IF), and on three dimensionless numbers: Re, Ra_S and Sc.

In other fluid dynamic problems, like the thermal driven cavity configuration, the difference in temperatures that causes the buoyancy forces is maintained constant during all the process. This is not the case in the situations considered in this section. The only buoyancy forces present here are due to concentration gradients. These forces are stronger at the beginning of the process, when the difference between the inlet concentration and the cavity concentration is higher. Their effect can change dramatically the trajectory of the jet from the inlet to the outlet, enhancing or worsening the transport of the contaminant. As the cavity is being cleaned, the gradients of concentration are reduced, and the buoyancy forces lose importance. At last, when the permanent state has been reached, C is uniformly equal to 1, so there is no longer a coupling between equations (1)–(3) and equation (5) and for a given geometrical disposition, the flow depends only on Re number. The instant in which the buoyancy forces are no longer important depends strongly on the case considered. In general, this transition from mixed convection to forced convection is smooth, but in some cases, a rather abrupt change is found.

The goal of this section is to provide a description of the cleaning times as a function of the flow parameters. All the aforementioned aspects cause this function to be quite complex, even for these isothermal cases, and a too high number of transient numerical simulations would be needed to obtain a full description of all possible situations, so only a part of them has been considered.

3.1. Simplified models

Before starting the discussion of the numerical results obtained, and for a better understanding of transient transport phenomena, it is convenient to consider two simple models that explain how the air replacement could ideally happen [1, 5, 22]: piston displacement flow model (PD) and perfectly mixed flow model (PM). In Fig. 5, predictions of both models can be compared with results obtained from the numerical simulations.

In the PD model, curve 'f', the new fluid ($C = 1$) is assumed to displace the contaminated fluid ($C = 0$) without mixing with it, in a piston-like fashion. Under this assumption,

$$\text{if} \quad \tau^* <= 1, \quad C_{avg} = \tau^*, \quad C_{min} = 0$$
$$\text{if} \quad \tau^* > 1, \quad C_{avg} = 1, \quad C_{min} = 1$$
$$\tau^*_{C_{avg}} = \tau^*_{C_{min}} = 0.95. \tag{7}$$

Therefore, flows behave in a piston displacement way ($C_{out} \approx 0, C_{avg} \approx \tau^*, C_{min} \approx 0$) only at the very beginning. Unfortunately, after a while, the fresh air from the inlet reaches the output so the PD model overpredicts the efficiency of the transport.

In the PM model, curve 'e', the flow is supposed to be such that the inlet jet perfectly mixes with the indoor air, so the concentration at the outlet is the same as the concentration at any point inside the enclosure. In this case,

$$C_{avg} = C_{min} = 1 - \exp(-\tau^*)$$
$$\tau^*_{C_{avg}} = \tau^*_{C_{min}} \approx 3. \tag{8}$$

This model provides a better explanation of the phenomena, but in general it still overpredicts the efficiency of the transport. The cases like 'a' and 'd', with C_{min} and C_{avg} plots below the PM line are by far more frequent. Since the mixing is not perfect, it is necessary that a substantial part of the contaminated fluid is pushed out without mixing with the fresh air in order to bring the transport performance over the PM line.

3.2. Influence of Ra_S

A parametric study was made with Ra_S numbers in the range between -7×10^6 and 7×10^6, keeping constant $Re = 30$ and $Sc = 1$, in order to determine $\tau^*_{C_{avg}}$ and $\tau^*_{C_{min}}$ as a function of Ra_S for both flow configurations. $\tau^*_{C_{min}}$ vs Ra_S is presented in Fig. 6. The plot for $\tau^*_{C_{avg}}$ shows a similar tendency, so it has not been included. A plot of the streamlines and concentration fields at $\tau^* = 1$ is presented in Fig. 7(a) for the DF configuration and in Fig. 7(b) for the IF configuration. The resulting flows can be classified in three groups:

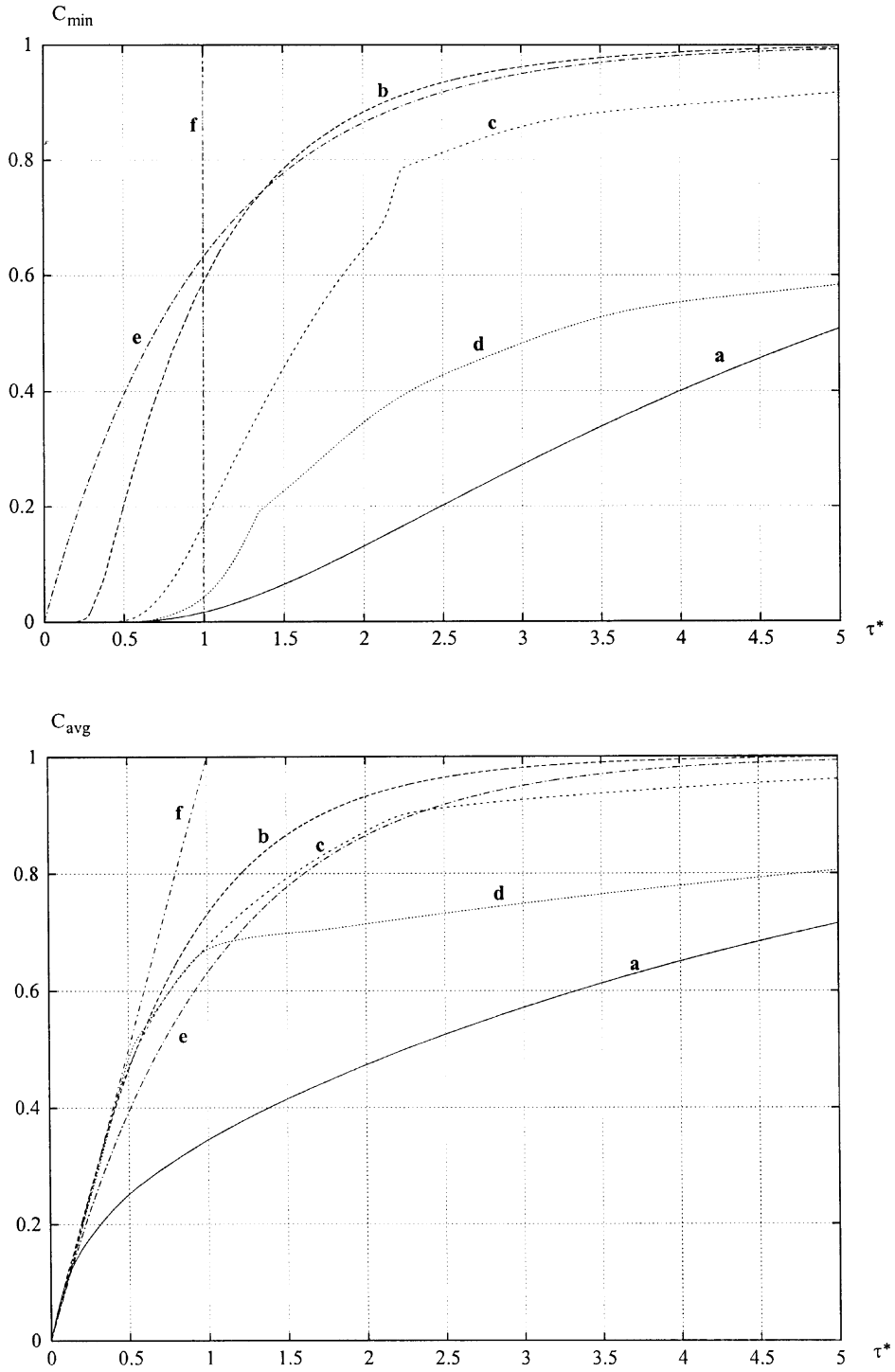

Fig. 5. C_{min} (top) and C_{avg} (bottom) vs τ^* for some isothermal $Sc = 1$, $Re = 30$, DF situations, to be compared with the predictions of PM and PD flow models. (a) $Re = 30$, $Ra_S = -7 \times 10^6$, $Sc = 1$; (b) $Re = 30$, $Ra_S = 7 \times 10^6$, $Sc = 1$; (c) $Re = 30$, $Ra_S = 3.5 \times 10^4$, $Sc = 2$; (d) $Re = 100$, $Ra_S = -3.5 \times 10^4$, $Sc = 2$; (e) PM flow model; (f) PD flow model.

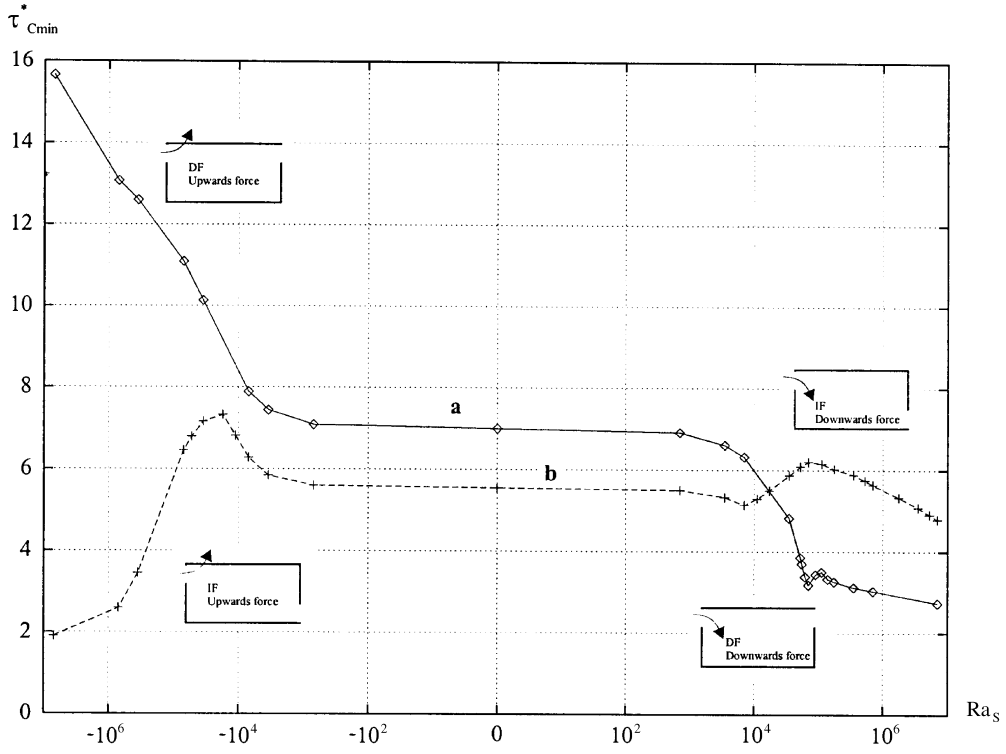

Fig. 6. $\tau^*_{C_{min}}$ in DF and IF dispositions, as a function of Ra_S number, for $Re = 30$ and $Sc = 1$ isothermal cases. (a) DF; (b) IF.

3.3. *Values of* Ra_S *smaller than* -10^3

In this range of values, DF configurations clean the cavity slower. This is due to the buoyancy force that pushes the jet upwards, confining it at the top of the cavity and causing stratification of the contaminant at the bottom, as can be seen in the iso-concentration field corresponding to this case in Fig. 7(a). This effect is important, since in the worst case considered the time required to clean the cavity is more than the double than in the non-buoyancy affected situation.

In IF configurations, Fig. 7(b), high negative values of Ra_S clean the cavity very efficiently. The heavier contaminant is pushed to the bottom and exits while the fresh air descends almost vertically, without mixing each other, almost like in the PD model. This effect is reduced as Ra_S approaches to zero and the cleaning time increases, reaching a local maximum around $Ra_S = -1.75 \times 10^4$.

In order to explain the presence of this relative maximum, the transient evolution for $Ra_S = -1.75 \times 10^4$ and $Ra_S = 0.0$ have been compared. In the latter, non-buoyancy-affected case, the transfer of momentum causes the apparition of a recirculation area, typical of a backward-facing-step like configuration. This recirculation enhances the mixing of the left bottom part of the cavity and thus reduces the cleaning time. This does not happen in the first, buoyancy affected case. For a certain range of buoyancy forces, the flow does not behave like in a PD model, and there is no good mixing, since the recirculation does not exist or it is weaker than in the non-buoyancy affected case. The combination of both effects causes the relative maximum.

3.4. *Values of* Ra_S *between* -10^3 *and* 10^3

For Ra_S numbers between -7×10^3 and 7×10^3, the influence of buoyancy forces is small and changes in Ra_S produce little effect, the curves are approximately horizontal. Changes in the streamline maps as time advances are smaller, since they are not due to the progressive decrease of the buoyancy force, but only to the effect of transient terms in momentum equations. IF configurations still perform better because they force the jet trajectory to be longer and enhance the mixing.

3.5. *Values of* $Ra_S > 10^3$

For significantly positive values of Ra_S, the buoyancy force pushes the jet to the bottom of the cavity. In IF

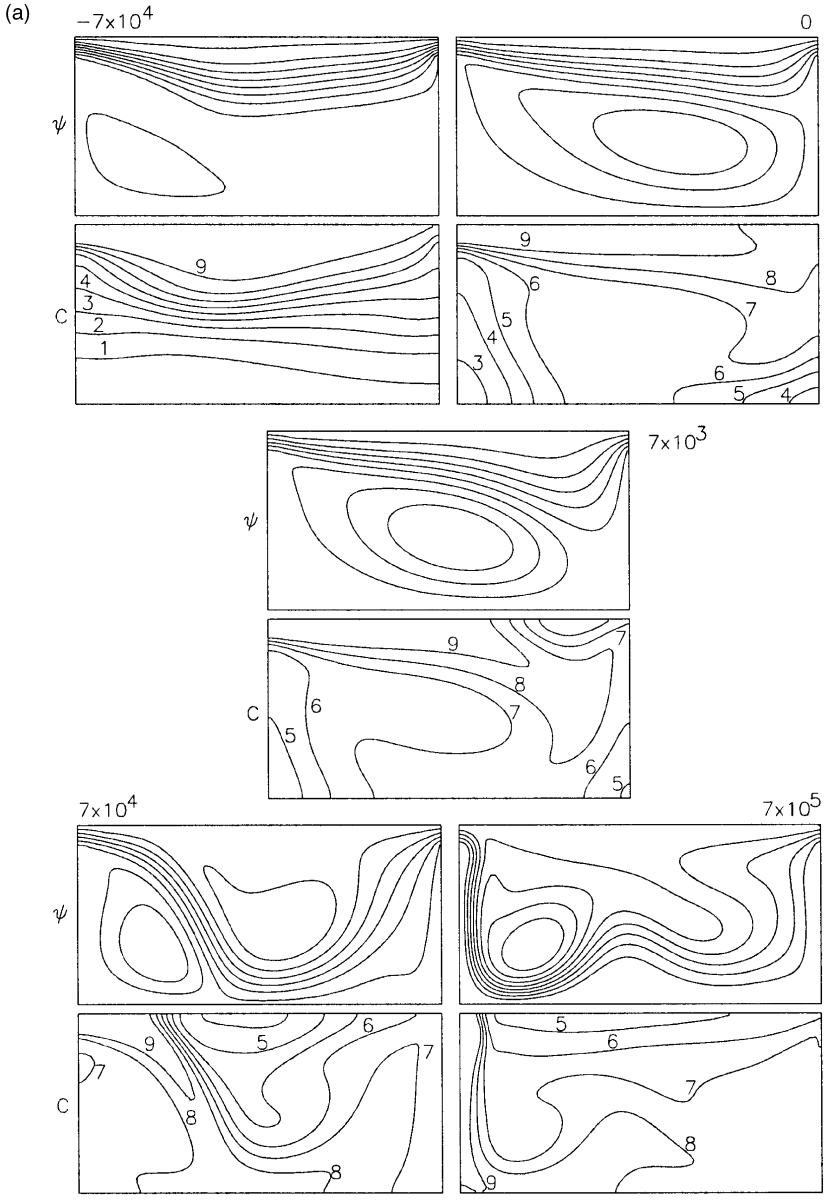

Fig. 7. Streamlines and iso-concentration maps after one air renovation ($\tau^* = 1$). The streamline values have been selected at equal intervals up to the maximum for each map. The written values of C have been multiplied by 10. The same criteria have been used elsewhere. (a) DF configurations. From left to right and top to bottom, $Ra_S = -7\times10^4, 0, 7\times10^3, 7\times10^4, 7\times10^5$. For $Ra_S = -7\times10^4$, note the concentration stratification and for positive Ra_S values, the enhancement of the transport due to the path that follows the jet as pushed downwards by the buoyancy force. (b) IF configurations. From left to right and top to bottom, $Ra_S = -7\times10^5, -1.75\times10^4$, $0, 7\times10^4, 7\times10^5$ and $\tau^* = 1$. For $Ra_S = -7\times10^5$, the velocity is almost vertical and the contaminant is pushed straight to the outlet. For $Ra_S = -1.75\times10^4$, the inlet is shortcutted to the outlet and two areas of low C values appear at the top right and the bottom left. For $Ra_S = 7\times10^5$, the jet is confined at the bottom of the cavity and the low C value area remains at the top.

configurations this allows the jet to remain close to the left wall first and close to the bottom later, reaching the outlet without providing good mixing. For this reason, for values of Ra_S greater than approximately 1.2×10^4, DF configurations give faster cleaning times. As seen in Fig. 7(a), for $Ra_S = 7\times10^5$, the effect is so extreme that light contaminant presents a certain stratification at the top of the cavity.

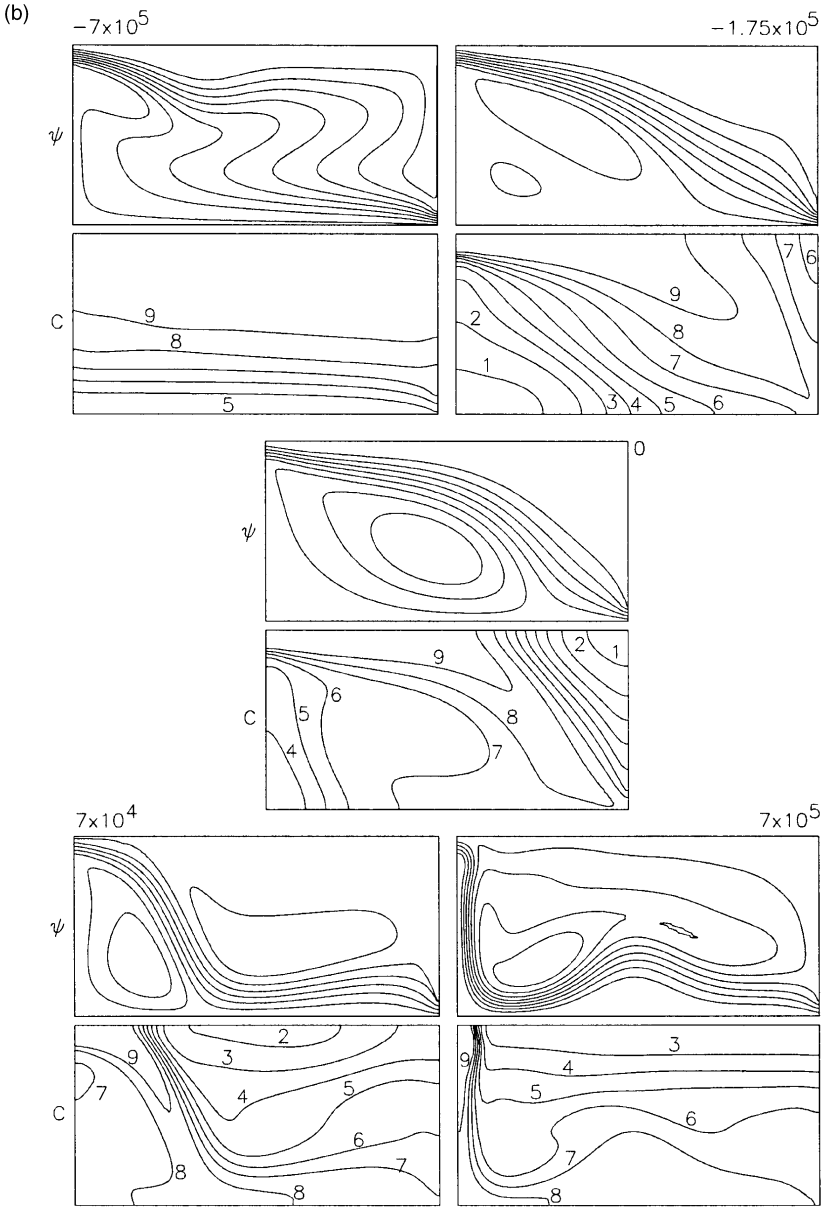

Fig. 7—*continued.*

For DF configurations, it is interesting to consider the flow history with certain detail. Figure 8 presents some plots of $C_{\min}$ vs τ^*, for DF situations of different Ra_S values, keeping $Re = 30$ and $Sc = 1$. In the plot corresponding to $Ra_S = 7 \times 10^4$ there is a sudden decrease in the slope of $C_{\min}$. This phenomena can also be found for a certain range of Ra_S values from approximately 7×10^3 to approximately 3.5×10^5. For 7×10^4, this transition occurs at $\tau^* = 3.2$, immediately after $C_{\min}$ reaches 0.95, and this is the reason why 7×10^4 is the local minimum of $\tau^*_{C_{\min}}$ vs Ra_S. The cause of this transition is analyzed in more detail in Fig. 9 where the streamline and iso-concentration maps corresponding to the transition and instants immediately before and after are represented. For $\tau^* = 3.1$, the zone of lower concentrations is at the right top and it is being cleaned fast by the jet. For $\tau^* = 3.2$, the concentrations in this zone have increased and are as high as the ones in the left bottom, while in the last plot, after the transition, the maximum (approximately 0.96) is at the left bottom of the cavity, in a low

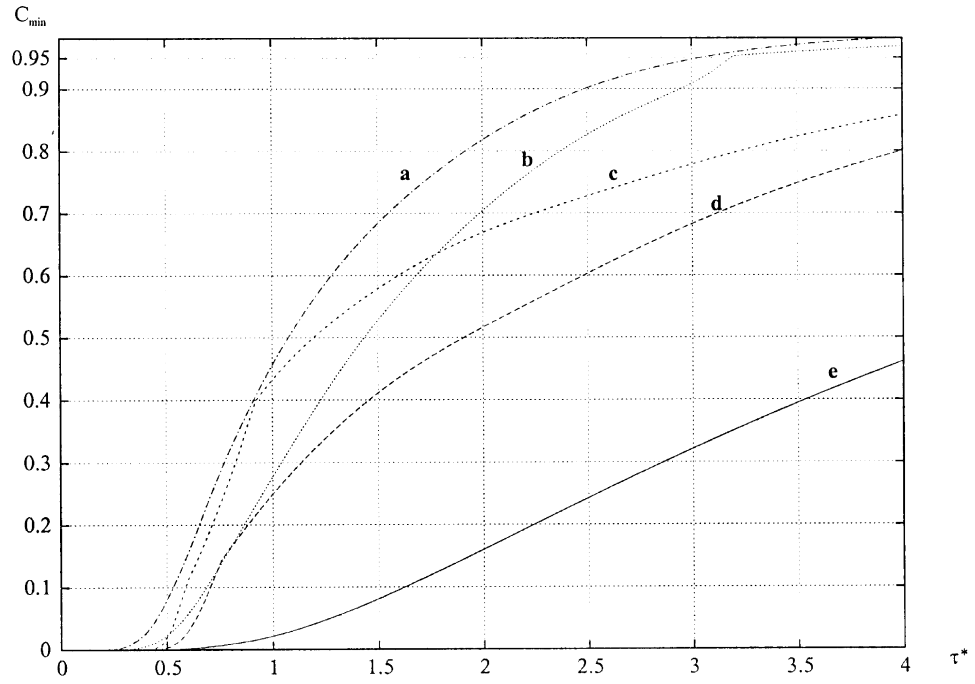

Fig. 8. C_{min} vs τ^* in different isothermal DF situations $Re = 30$, $Sc = 1$. (a) $Ra_S = 7 \times 10^5$; (b) $Ra_S = 7 \times 10^4$; (c) $Ra_S = 7 \times 10^3$; (d) $Ra_S = 0$; (e) $Ra_S = -7 \times 10^5$.

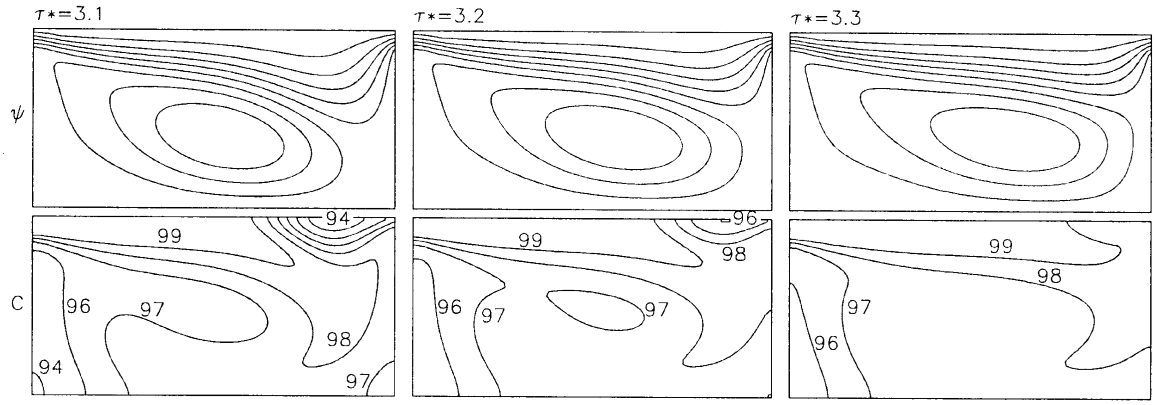

Fig. 9. Transient evolution of the isothermal DF, $Re = 30$, $Sc = 1$, $Ra_S = 7 \times 10^4$ case. The change in the minimum position (from top left to bottom right) explains the discontinuity in the slope of C_{min} vs τ^*.

velocity area, causing the rate of minimum-decrease to be very slow for $\tau^* >= 3.2$.

3.6. *Influence of* Sc

In order to determine the effect of the contaminant molecular diffusivity, a parametric study has been made for DF configurations, for three *Sc* numbers (0.25, 1, 2.0) and Ra_S numbers in the range of -10^6–10^6, keeping constant $Re = 30$. The values of $\tau^*_{C_{min}}$ vs Ra_S are represented in Fig. 10; $\tau^*_{C_{avg}}$ has a similar tendency and it is not represented.

In the cases that present stratification, and in general, in all the poor ventilated cases, diffusion plays a more relevant paper in the transport process, and changes in *Sc* number have more influence. As discussed in the previous

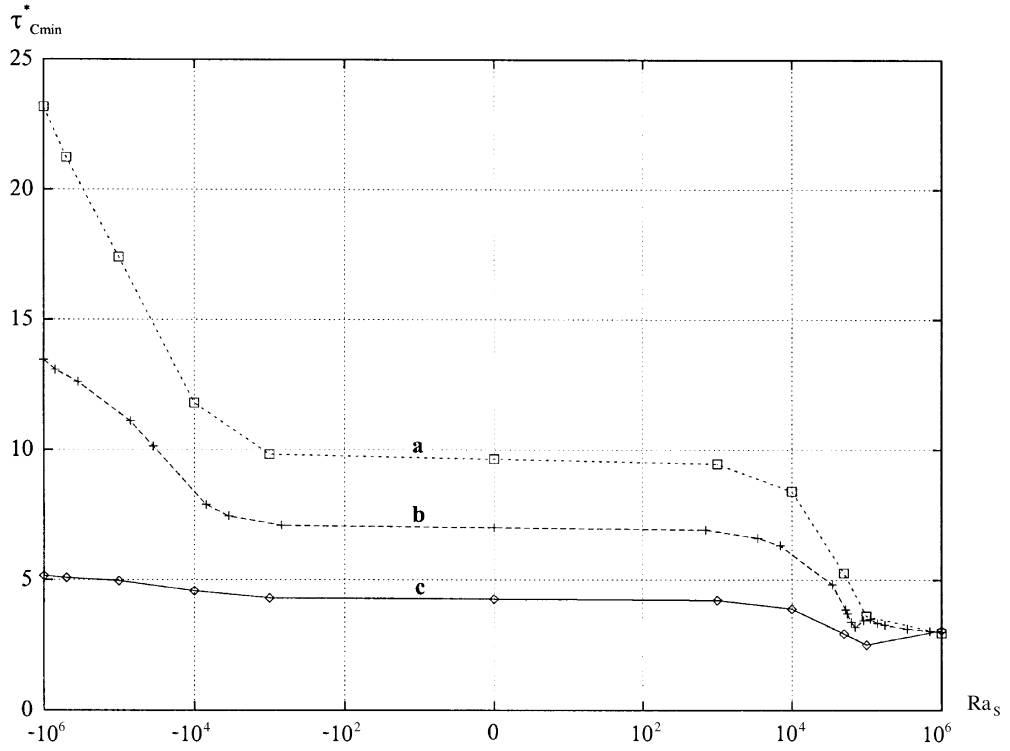

Fig. 10. $\tau^*_{C_{min}}$ in isothermal DF configurations, $Re = 30$, for different Sc and Ra_S, numbers. For negative Ra_S numbers (left part of the plot), there is a stratification of the contaminant that causes the diffusion transport to be more important, and consequently increases the effect of Sc numbers. (a) $Sc = 2.0$; (b) $Sc = 1.0$; (c) $Sc = 0.25$.

section, this is the case in negative Ra_S numbers part of Fig. 6. On the other hand, for positive Ra_S numbers, and in general for all the well ventilated cases, diffusion is less important and small changes in Sc may have little or no effect over the cleaning times. The abrupt changes in the slope of C_{min} vs τ^* that were discussed in the previous section for $Sc = 1$, are more evident for $Sc = 2$, as can be seen in Fig. 3b.

3.7. *Influence of* Re

The effect of changing Re for a DF situation with $Sc = 1$ has been studied. The results obtained are summarized in Fig. 11. As Re increases, two effects can be observed:

(i) The time to complete each air renovation decreases. As we are considering τ^* to be the time scale, for higher Re values the physical time elapses faster, and diffusion has less importance. Moreover, the path followed by the streamlines from the inlet to the outlet changes as the speed at the inlet is higher. In general, the tendency is to close the streamlines to the walls. Both effects cause worse mixing and increase the number of air renovations required to clean the cavity. For $Ra_S = 10^6$, these effects are not so clear and the cleaning times remain almost independent of Re in the range of 10–50. This may be due to the extremely good mixing that this configuration provides, as can be seen in Fig. 12, where its transient evolution is shown.

(ii) Buoyancy has less importance in the balance of the forces that act over the jet. For Ra_S between -10^5 and 10^5, the increase of Re causes $\tau^*_{C_{min}}$ to be almost independent of Ra_S. This is not the case for $Ra_S = -10^6$ and $Ra_S = 10^6$, the convergence over the non-buoyancy affected cases will probably appear for higher Re numbers.

4. Non-isothermal situations

The cases here under consideration have one added feature compared to those considered in Section 3: the presence of a thermal field generated by a difference of temperatures that is maintained constant. As said in the introduction, these situations are referred as double

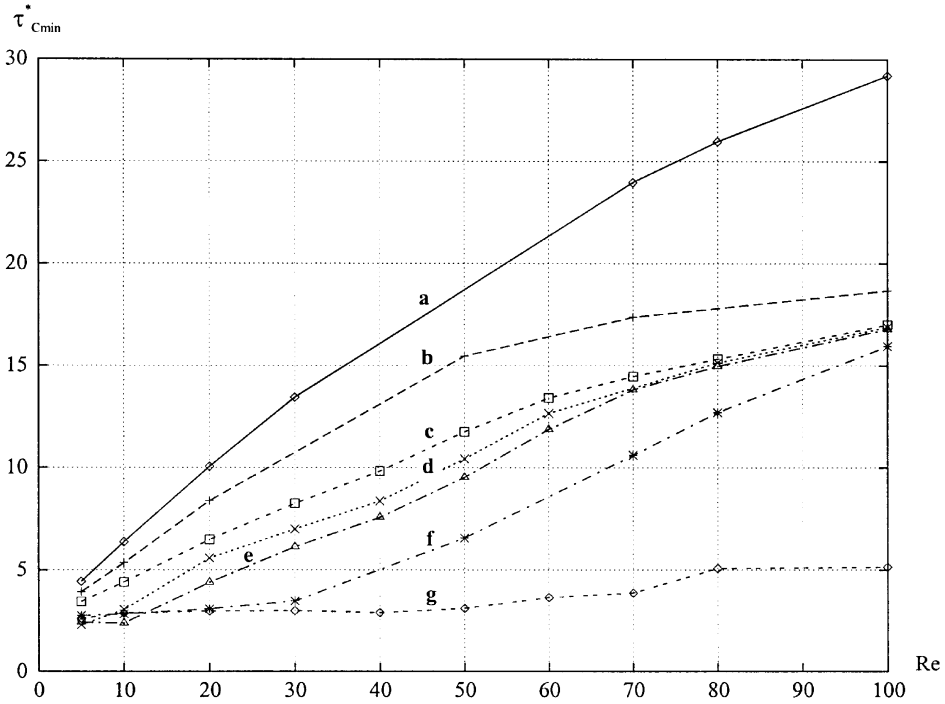

Fig. 11. $\tau^*_{C_{min}}$ vs Re in isothermal DF configurations for different Ra_S numbers. (a) $Ra_S = -10^6$; (b) $Ra_S = -10^5$; (c) $Ra_S = -10^4$; (d) $Ra_S = 0$; (e) $Ra_S = 10^4$; (f) $Ra_S = 10^5$; (g) $Ra_S = 10^6$.

diffusion problems. The buoyancy forces are now due to two reasons: differences of concentration (that in our case tend to vanish as the cavity is being cleaned) and differences of temperature. The transport process depends on one more dimensionless number, Ra_T. As mentioned in Section 2, for a given Ra_T two boundary conditions (positive or negative temperature difference) and two initial conditions (steady or static) have been considered.

Here, when the cavity has been cleaned, the temperature field still generates buoyancy forces and the flow in the permanent state depends on Re and on Ra_T. The goal of this section is to illustrate with some examples the different effects that temperature field may have over the transport process. Only DF situations will be discussed, because in these cases the buoyancy forces have been found to be specially relevant.

The temperature field has two effects over the flow. First, the temperature inlet T_{in} generates a buoyancy force that can be upwards ($T_{in} = 1$) or downwards ($T_{in} = 0$). This force has to be added to the buoyancy force due to the inlet concentration ($C_{in} = 1$). Second, the difference of temperature of the walls that tends to induce buoyancy driven velocities that enhance the mixing process. This second effect is specially relevant in the cases where the buoyancy forces due to concentration tend to produce stratification.

4.1. *Negative* Ra_S *number in DF configuration*

Different DF situations with $Ra_T = 10^5$, $Ra_S = -10^5$, $Sc = 1$ and $Re = 30$ have been simulated. Their C_{min} vs τ^* curves have been plotted in Fig. 13. The situations 'a' and 'b' have also been plotted to be compared with the rest of the set. Curve 'a' corresponds to the non-buoyancy affected case, $Ra_S = Ra_T = 0$, while curve 'b' corresponds to the previously discussed $Ra_T = 0$, $Ra_S = -10^5$ situation. A negative temperature difference ($T_l = T_{in} = 0$, $T_r = 0$) has been imposed in cases 'c' and 'd' and a positive temperature difference ($T_l = T_{in} = 0$, $T_r = 1$) in case 'e'. Static initial conditions have been imposed in cases 'd' and 'e' and steady initial conditions in case 'c'.

In situations 'c' and 'd', the buoyancy force due to temperature gradient cooperates with the force due to concentration gradient at the inlet region, pushing the jet upwards and confining it to the top of the cavity. Thus, by comparison with the isothermal negative Ra_S situations, $\tau^*_{C_{min}}$ could be expected to be larger for cases 'c' and 'd' than for the reference situation 'b', where there is only a concentration force. Numerical experiments show that the buoyancy effect at the inlet is relevant only at the beginning, because later the secondary flow caused by the differences of wall temperature enhances the transport process. This is clearly visible in the transient evolution of case 'c' (Fig. 14). The vertical velocity at the cold right

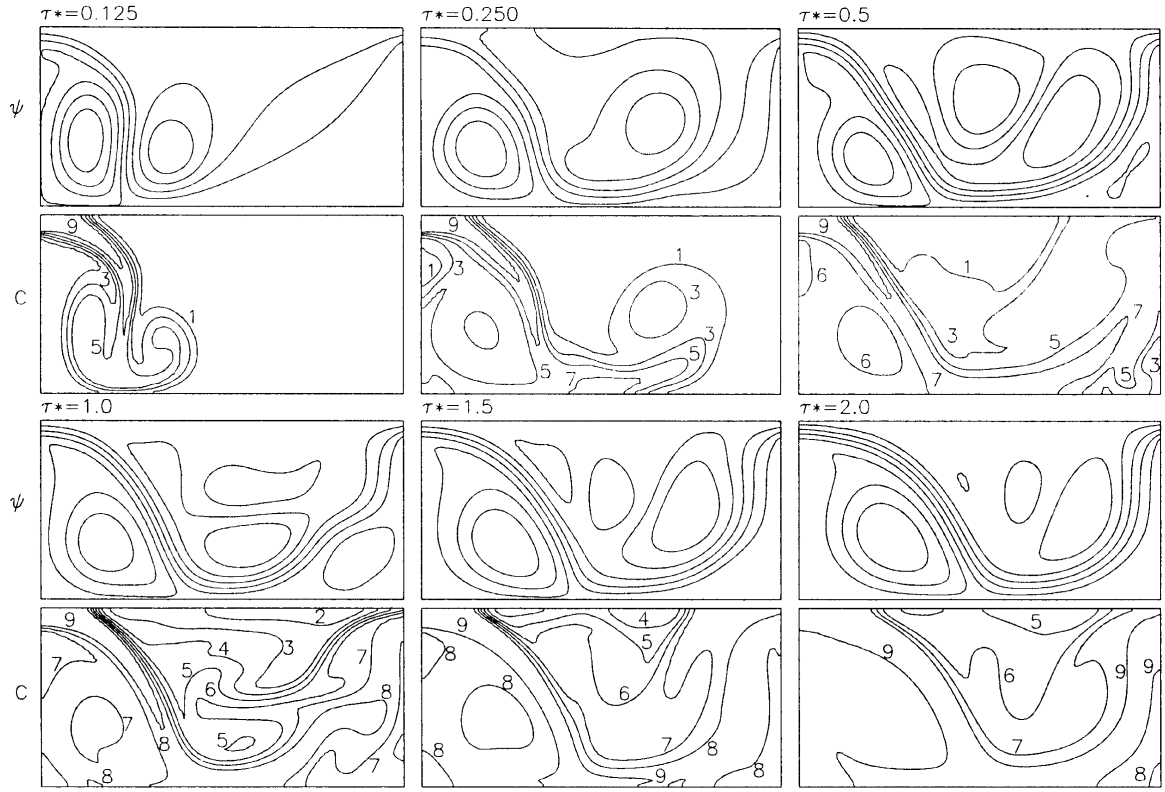

Fig. 12. Transient evolution of the isothermal DF case, for $Re = 100$, $Sc = 1$, $Ra_S = 10^6$. Streamlines and isoconcentration maps for $\tau^* = 0.125, 0.250, 0.5, 1.0, 1.5, 2.0$ (from top to bottom and left to right).

wall convects the low C regions downwards, where they are mixed with the high C areas, increasing C_{min}. The difference between cases 'c' and 'd' is their initial condition: steady and static thermal driven flow, respectively. As expected, this difference is relevant at the beginning of the process but has little importance afterwards.

In case 'e', the temperature gradient force counteracts the effect of the concentration gradient force. There is a buoyancy driven flow from the area close to the right wall to the outlet. Both effects tend to push the inlet jet down, counteracting the buoyancy effect due to the concentration gradient and enhancing the transport process.

As a conclusion for this set of situations, we can state that the temperature gradient helps to the transport process, although its importance depends on the sign of the temperature difference.

4.2. *Positive* Ra_S *number in DF configuration*

A DF situation like the previous, but with $Ra_S = 10^5$ has been considered. The corresponding transient evolutions have been plotted in Fig. 15. The non-buoyancy-affected situation and a situation with buoyancy force due only to concentration, have been also plotted as references (cases 'a' and 'b'). Here, the buoyancy force due to concentration gradient tends to push the jet down, causing a well mixed flow and a short cleaning time, this is why 'b' performs better than 'a'.

Only a negative temperature difference has been considered here (cases 'c' and 'd'). Unlike in the previous situation, here the bad effects of the temperature field are more important than the good ones. The global result is a cleaning time shorter than in the non-buoyancy-affected situation, but longer than in the situation only affected by concentration gradient.

Like in the previous section, the difference between 'c' and 'd' is the initial condition. As can be seen in Fig. 15, in this case the initial condition has more effect over the flow history. Both transient evolutions have been plotted in Fig. 16.

5. Conclusions

The transient removal of a contaminant from an enclosure has been studied by performing many transient numerical simulations in order to determine $\tau^*_{C_{min}}$, the

Fig. 13

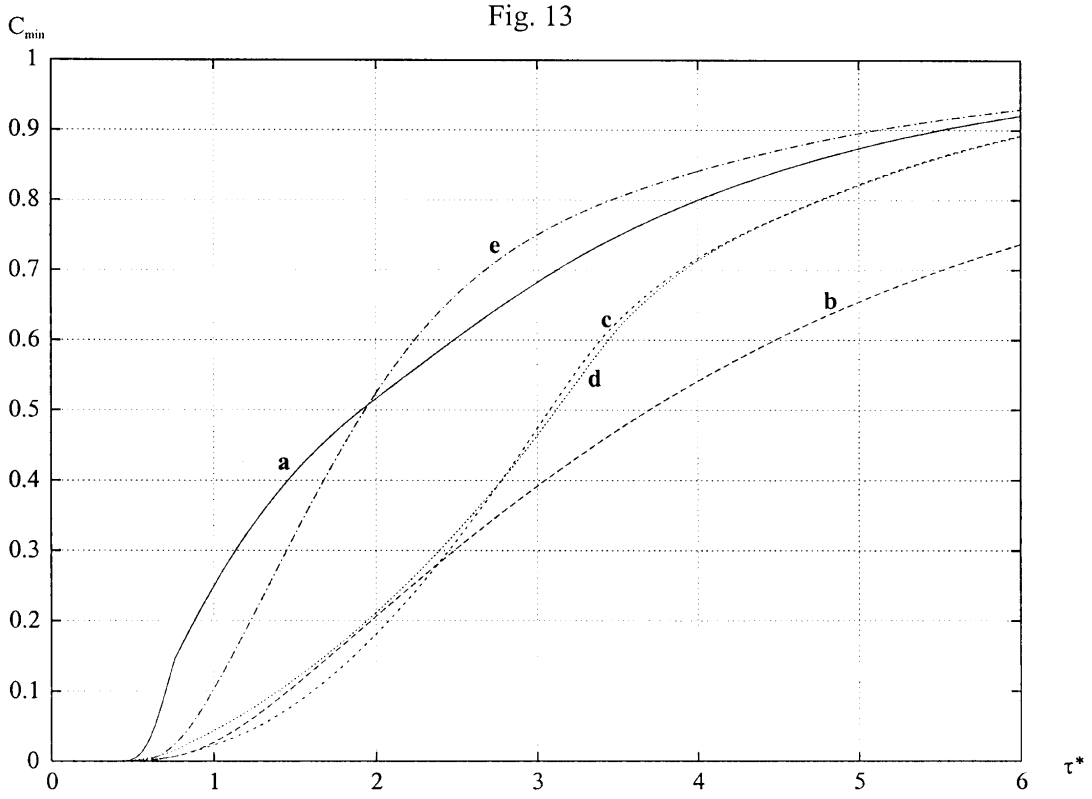

Fig. 13. C_{min} vs τ^* for DF configurations with $Re = 30$ and $Sc = 1.0$. (a) Non-buoyancy-affected, $Ra_T = 0$, $Ra_S = 0$; (b) isothermal, $Ra_T = 0$, $Ra_S = -10^5$; (c) $Ra_T = 10^5$ (negative difference), $Ra_S = -10^5$. Initial conditions: steady thermal driven flow; (d) $Ra_T = 10^5$ (negative difference), $Ra_S = -10^5$, initial conditions: static; (e) $Ra_T = 10^5$ (positive difference), $Ra_s = -10^5$, initial conditions: static.

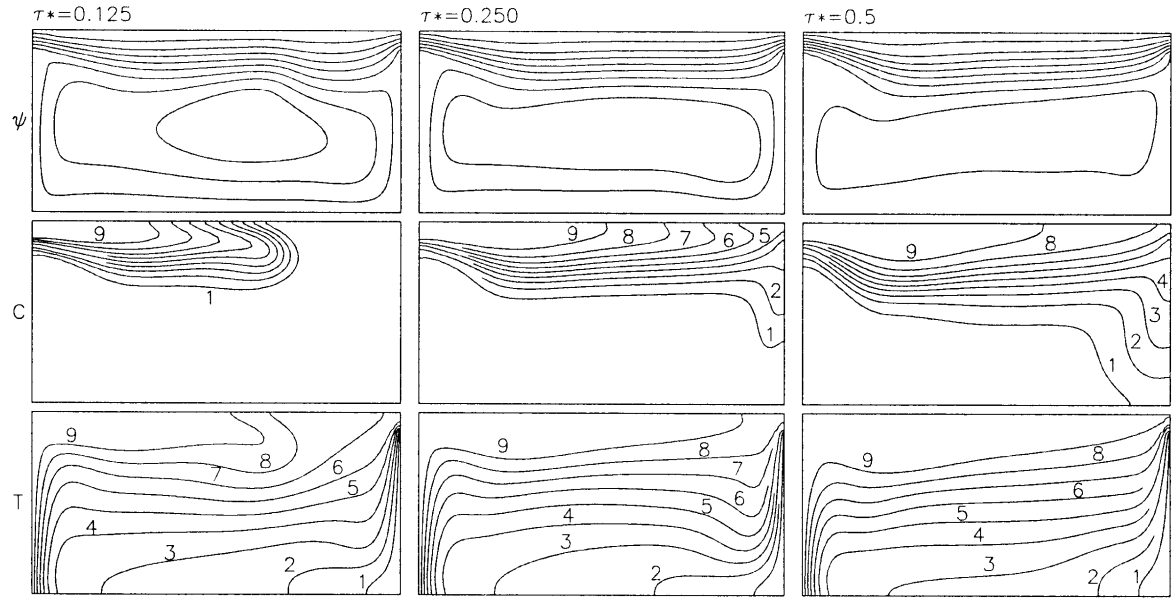

Fig. 14. Transient evolution of a DF with $Ra_T = 10^5$ (negative temperature difference), $Ra_S = -10^5$; $Re = 30$; $Sc = 1$. Initial conditions: steady thermal driven flow. $\tau^* = 0.125, 0.250, 0.5$ (from left to right).

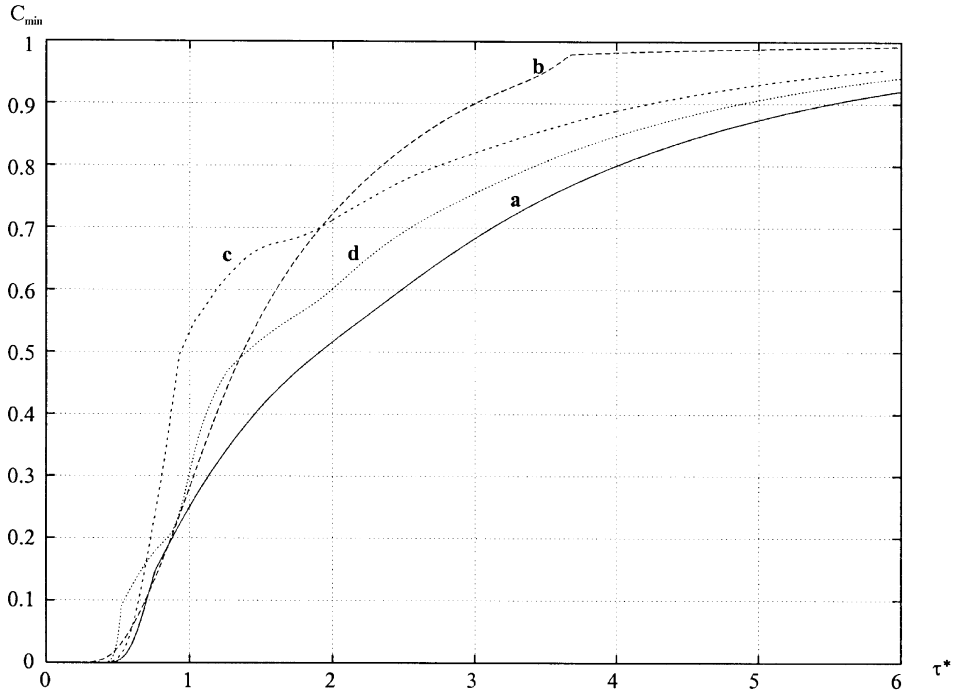

Fig. 15. C_{min} vs τ^* for DF configurations with $Re = 30$ and $Sc = 1.0$. (a) Non-buoyancy-affected, $Ra_T = 0$, $Ra_S = 0$; (b) Isothermal, $Ra_T = 0$, $Ra_S = 10^5$; (c) $Ra_T = 10^5$ (negative difference), $Ra_S = 10^5$, initial conditions: steady; (d) $Ra_T = 10^5$ (negative difference), $Ra_S = 10^5$, initial conditions: static.

number of air renovations required to clean the cavity up to a 5% of its final (clean) value. Special attention has been paid to the buoyancy effects caused by concentration and temperature gradients. A parametric study has been made for isothermal situations. The effect of temperature gradients on some significant situations has been determined.

In general, for the isothermal cases studied, the buoyancy effect caused by the density of the contaminant has an important influence over the flow, increasing or decreasing dramatically $\tau^*_{C_{min}}$. In cases where the buoyancy force causes a stratification of the contaminant and, in general, in all the poor ventilated situations, an important part of the transport process is due to diffusion. This causes the contaminant diffusivity to be specially significant. In the opposite situations, where the buoyancy effect causes the flow to clean the cavity efficiently, the contaminant diffusivity has very little influence. In general, as Re increases, the influence of Ra_S becomes smaller, and $\tau^*_{C_{min}}$ increases because the mixing is worse. In some cases (DF configuration, $Ra_S = 10^6$), in a quite wide range of Re, $\tau^*_{C_{min}}$ remains almost equal.

The presence of a temperature gradient makes more complex the transport process. In some poor ventilated cases, temperature gradients enhance mixing and decrease $\tau^*_{C_{min}}$, but in others where the buoyancy effects due to concentration gradients cause the flow to be efficient, the effect can be the opposite.

For the range of dimensionless values studied, it is essential to take into consideration the effects of buoyancy caused by temperature and concentration gradients, in order to make reasonably accurate predictions of the flow histories and cleaning times. Due to the complexity of the phenomena involved, it will be difficult to find compact analytical expressions to predict the cleaning time as a function of all the parameters involved.

In the near future, this work will be oriented in obtaining the most efficient inlet and outlet port placements and directions, as well as the flow rates required to displace different contaminants in a given time. It will be necessary to investigate the flow patterns involved in turbulent three-dimensional situations. Although the extension to three dimensions is straightforward, the dramatic increase in CPU time is still a limitation in problems like the one here considered, where a large number of parameters are involved and many simulations have to be done. In order to deal with turbulent flows, the implementation of two equations k–e turbulence models (using wall functions or in its more general form of low-Reynolds-number k–e models) will be made. Exper-

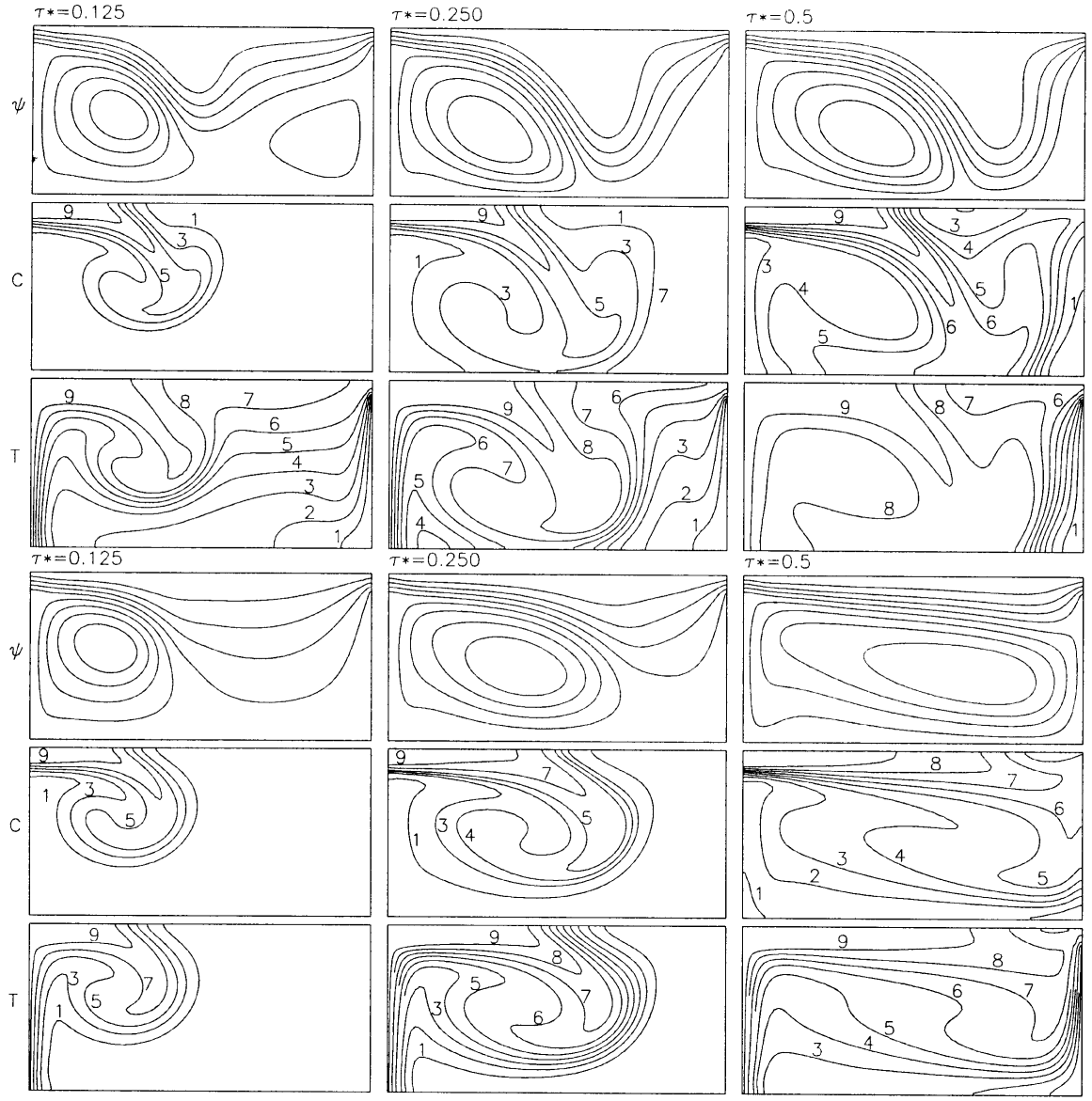

Fig. 16. Transient evolution of the DF, $Ra_T = 10^5$ (negative difference), $Ra_S = -10^5$, $Re = 30$, $Sc = 1$. Top: steady flow initial conditions. Bottom: static initial conditions.

imental measures will be required to validate the turbulence models in this double-diffusive flows.

Acknowledgements

This research has been supported by 'Comisión Interministerial de Ciencia y Tecnologia' (project no. TIC95-0724) and by the 'Comissionat per a Universitats i Recerca de la Generalitat de Catalunya' (Ref. FI95-3.322).

References

[1] Awbi HB. Ventilation of Buildings. London: E&FN SPON, 1991.
[2] Fang, Grot R A. Numerical simulation of the performance of building ventilation systems. ASHRAE Transactions 1990;96(2):361–6.
[3] Murakami S, Kato S, Suyama Y. Numerical study of flow and contaminant diffusion field as affected by flow obstacles in conventional-flow-type clean room. ASHRAE Transactions 1990;96(2):343–55.
[4] Kato S, Murakami S, Nagano S. Numerical study on

diffusion in a room with a locally balanced supply–exhaust airflow rate system. ASHRAE Transactions 1992;98(1):218–38.
[5] Lage JL, Bejan A, Anderson R. Efficiency of transient contaminated removal from a slot ventilated enclosure. Int J Heat Mass Transfer 1991;34:2603–15.
[6] Lage JL, Bejan A, Anderson R. Removal of contaminant generated by a discrete source in a slot ventilated enclosure. Int J Heat Mass Transfer 1992;35:1169–80.
[7] Gebhart B, Pera L. The nature of vertical natural convection flows resulting from the combined buoyancy effects of thermal and mass diffusion. Int J Heat Mass Transfer 1971;14:2025–50.
[8] Bergman TL, Ungan A. Experimental and numerical investigation of double-diffusive convection induced by a discrete heat source. Int J Heat Mass Transfer 1986;29:1695–709.
[9] Lee JW, Hyun JM. Double-diffusive convection in a rectangle with opposing horizontal gradients of temperature and concentration. Int J Heat Mass Transfer 1990;33:1619–32.
[10] Hyun JM, Lee JW. Double-diffusive convection in a rectangle with cooperating horizontal gradients of temperature and concentration. Int J Heat Mass Transfer 1990;33:1605–17.
[11] Han H, Kuehn TH. Double diffusive natural convection in a vertical rectangular enclosure—I. Experimental study. Int J Heat Mass Transfer 1991;34:449–59.
[12] Han H, Kuehn TH. Double diffusive natural convection in a vertical rectangular enclosure—II. Numerical study. Int J Heat Mass Transfer 1991;34:461–71.
[13] Viskanta R, Weaver JA. Natural convection due to horizontal temperature and concentration gradients—1. Variable thermophysical property effects. Int J Heat Mass Transfer 1991;34:3107–20.
[14] Weaver JA, Viskanta R. Natural convection due to horizontal temperature and concentration gradients—2. Species interdiffusion, Soret and Dufour effects. Int J Heat Mass Transfer 1991;34:3121–33.
[15] Katsuyoshi K, Ozoe H. Experimental and numerical analyses of double diffusive natural convection heated and cooled from opposing vertical walls with an initial condition of a vertically linear concentration gradient. Int J Heat Mass Transfer 1993;36:2125–34.
[16] Béghein C, Haghighat F, Allard F. Numerical study of double-diffusive natural convection in a square cavity. Int J Heat Mass Transfer 1992;35:833–46.
[17] Fusegi T, Hyun JM, Kuwahara K, Farouk B. A numerical study of three-dimensional natural convection in a differentially heated cubical enclosure. Int J Heat Mass Transfer 1991;34:1543–57.
[18] Ivancic A, Oliva A, Pérez-Segarra CD, Schweiger H. Three-dimensional numerical study of mixed convection in cylindrical cavities. In Lewis RW, editor. Numerical Methods in Thermal Problems 1993;VIII(1):561–72. Swansea.
[19] Patel VC, Rodi W, Scheuerer G. Turbulence models for near-wall and low Reynolds number flows : a review. AIAA J 1985;23:1308–19.
[20] Pérez-Segarra CD, Oliva A, Costa M, Escanes F. Numerical experiments in turbulent natural and mixed convection in internal flows. Int J Num Meth Heat Fluid Flow 1995;5:13–33.
[21] Grew KE, Ibbs TL. Thermal diffusion in gases. London: Cambridge, 1952.
[22] Anderson R, Mehos M. Evaluation of indoor air pollutant control techniques using scale experiments. Engineering Solutions to Indoor Air Problems, Proc. ASHRAE Conf. IAQ 88. Atlanta, Georgia, 1988, pp. 193–208.
[23] Van Doormaal JP, Raithby GD. Enhancements of the SIMPLE method for predicting incompressible fluid flows. Numerical Heat Transfer 1984;7:147–63.
[24] Patankar SV. Numerical heat transfer and fluid flow. New York : McGraw-Hill, 1980.
[25] Gaskell PH, Lau AKC. Curvature-compensed convective transport : SMART, a new boundedness-preserving transport algorithm. International Journal for Numerical Methods in Fluids 1988;8:617–41.
[26] Scheneider GE, Zedan M. A modified strongly implicit procedure for the numerical solution of field problems. Numerical Heat Transfer 1981;4:1–19.
[27] De Vahl Davis G, Jones IP. Natural convection in a square cavity : a comparison exercise. International Journal for Numerical Methods in Fluids 1983;3:227–48.
[28] Fu W-S, Kau T-M, Shieh W-J, Transient laminar natural convection in an enclosure from steady flow state to stationary stage. Numerical Heat Transfer 1990;18(A):189–212.